

Technische Universität Braunschweig
Institut für Flugantriebe und Strömungsmaschinen (IFAS)
Jun.-Prof. Federica Ferraro
Course: Numerical Simulation of reactive flows
Winter Semester 2025/2026

Report 2: Counterflow flame simulations with OpenFOAM

SHUBHAM KUMAR, Matriculation number: 5547548

Course of study: Computational Sciences in Engineering (CSE)

1 Introduction

The report presents an analysis of two-dimensional reacting flows using the open-source CFD framework OpenFOAM. A counterflow flame configuration is considered, where opposing fuel and oxidizer streams interact to form a stabilized laminar flame near a stagnation plane. This configuration provides a canonical test case for investigating the coupling between fluid dynamics, chemical kinetics, and heat release.

This reports to assess mesh sensitivity, analyze the influence of inlet velocity, pressure, fuel composition, and inlet temperature, and to compare flame characteristics for different fuel mixtures. The study also examines the flame structure using temperature, species mass fractions, Bilger mixture fraction, and heat release rate as key diagnostic quantities.

1.1 Problem Description

The computational setup consists of a two-dimensional counterflow configuration, in which a fuel stream and an oxidizer stream enter the domain from opposite sides along the axial (x) direction.

The domain spans $0 \leq x \leq 0.02$ m in the axial direction and $-0.01 \leq y \leq 0.01$ m in the transverse direction. The flow is assumed laminar, and all simulations are performed using the `reactingFoam` solver in OpenFOAM, which solves the compressible Navier–Stokes equations coupled with species transport and finite-rate chemical reactions.

Air is used as the oxidizer in all cases and is modeled as a mixture of oxygen and nitrogen with the following mass fractions:

$$Y_{\text{O}_2} = 0.233, \quad Y_{\text{N}_2} = 0.767$$

Three different fuel mixtures are investigated in this study:

- **Fuel 1:** Methane–nitrogen mixture consisting of 85% CH_4 and 15% N_2 by volume.

$$Y_{\text{CH}_4} = 0.764, \quad Y_{\text{N}_2} = 0.236$$

- **Fuel 2:** Methane–steam mixture consisting of 85% CH_4 and 15% H_2O by volume.

$$Y_{\text{CH}_4} = 0.834, \quad Y_{\text{H}_2\text{O}} = 0.166$$

- **Fuel 3:** Diluted methane mixture consisting of 80% CH_4 , 10% CO_2 , and 10% H_2O by volume.

$$Y_{\text{CH}_4} = 0.674, \quad Y_{\text{CO}_2} = 0.232, \quad Y_{\text{H}_2\text{O}} = 0.095$$

2 Exercise (a): Mesh Refinement Study

Mesh refinement study was performed for the two-dimensional counterflow flame configuration to assess mesh sensitivity of the solution. Three structured meshes were considered, denoted as Mesh A, Mesh B, and Mesh C, with increasing resolution in the axial (x) direction while keeping the transverse resolution fixed. Figure 1 and Table 1 shows the computational grids (meshA, meshB, meshC) used in this study. The mesh parameters for the three cases are summarized as follows:

- Mesh A: $150 \times 40 \times 1$.
- Mesh B: $250 \times 40 \times 1$.
- Mesh C: $350 \times 40 \times 1$.

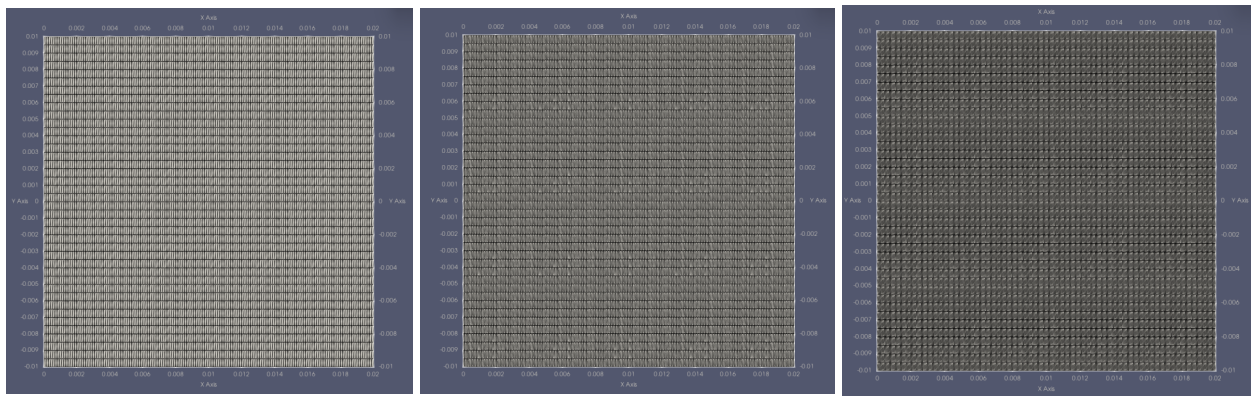


Figure 1: Computational grid for mesh A (left), mesh B (center), mesh C (right)

Table 1: Mesh specifications for convergence study

	Total cells	Max aspect ratio	Cell type
Mesh A	6000	3.75	Hexahedral
Mesh B	10000	6.25	Hexahedral
Mesh C	14000	8.75	Hexahedral

2.1 Simulation Steps

Three progressively refined structured meshes were employed to assess the mesh sensitivity. The meshes differed only in the axial (x) direction resolution as defined in *system/blockMeshDict* file. All simulations were performed under identical operating conditions, with equal and opposite inlet velocities of $\pm 0.15m/s$ as defined in *0/U* file, identical inlet temperatures defined in *0/T*, and a pressure of 1 bar defined in *0/P* files respectively. Fuel mass fractions were updated, in the respective specie files in folder 0, and also update the fuel-air composition in the *system/FOBilgerMixtureFraction*.

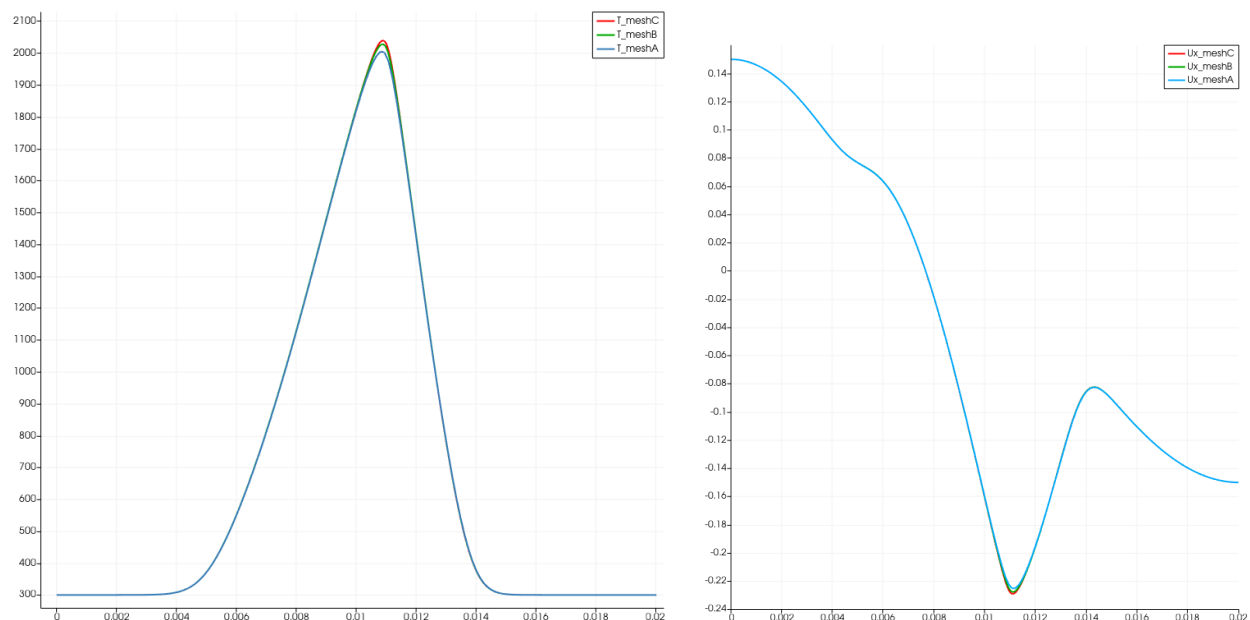
Each case was initialised using the same initial fields and advanced in time using the `reactingFoam` solver until a steady flame structure was obtained. After convergence, centerline profiles of tem-

2.2 Results and Discussion

perature and axial velocity were extracted along the x -direction for quantitative comparison as summarised in next section, using sampling setup in *system/sample*.

2.2 Results and Discussion

The influence of mesh refinement on the predicted flame structure is shown in Figure 2, which shows the centerline axial velocity $U_x(x)$ (Fig.2b) and temperature $T(x)$ profiles (Fig.2a) for Mesh A, Mesh B, and Mesh C (left plot).



(a) Centerline temperature vs axial-direction profiles, $T(x)$. (b) Centerline axial velocity $U_x(x)$ showcasing stagnation plane convergence

Figure 2: Mesh convergence study results, for Mesh A, Mesh B, and Mesh C

Temperature Distribution (Fig.2a)

The coarsest mesh (Mesh A) predicts a slightly broader flame region and a marginally lower peak temperature, which is indicative of numerical smearing of steep thermal gradients. As the mesh is refined, the temperature gradient across the flame zone becomes sharper and the peak temperature increases slightly, reflecting improved resolution of the reaction zone.

The temperature profiles obtained with Mesh B and Mesh C are nearly identical in both peak value and flame location, demonstrating that the solution is effectively grid-independent beyond Mesh B. Consequently, Mesh B provides an optimal compromise between numerical accuracy and computational cost and is therefore selected for all subsequent simulation tasks later exercises.

Stagnation Plane Location (Fig.2b)

The stagnation plane is identified as the axial location where the streamwise velocity component

2.2 Results and Discussion

U_x changes sign. As shown in Figure 2b, all three meshes predict a clear zero-crossing of U_x at approximately axial location 0.00766, the presence of a well-defined stagnation plane. With mesh refinement, the location of this zero-crossing converges, and the velocity profiles obtained with Mesh B and Mesh C nearly overlap. This indicates that the opposing jet interaction and momentum balance are sufficiently resolved on Mesh B, while Mesh A exhibits minor deviations due to increased numerical diffusion.

Determination of Stagnation Plane Location

The axial position of the stagnation plane was determined from the centerline axial velocity profile. After reaching steady state, the centerline data were extracted using the OpenFOAM postProcess file in the latest time folder `postProcessing/sample/0.5/.xy`, which contains sampled centerline quantities including the axial velocity component U_x . The stagnation plane location was identified as the axial position where U_x changes sign. A linear interpolation between the two neighbouring points surrounding $U_x = 0$ was used to compute the precise stagnation location.

The stagnation plane location converges with mesh refinement, with only marginal differences between Mesh B and Mesh C. Difference between Mesh B and Mesh C: $\approx 1.95 \times 10^{-6}$ m (0.0002 %). That is extremely small, confirming stagnation plane convergence. The resulting stagnation plane positions for the three meshes are listed in Table 2.

Table 2: Axial position of stagnation plane for different mesh resolutions

Mesh	$x_{\text{stagnation}}$ (m)
Mesh A	0.0076631
Mesh B	0.0076633
Mesh C	0.0076613

3 Exercise (b): Effect of Inlet Velocity

In this exercise, by varying the inlet velocity while keeping all other parameters fixed as previous exercise (a), the effect of flow-induced strain on flame thickness, peak temperature, and flame location have been systematically investigated.

3.1 Simulation Steps

Three simulations were compared with different magnitudes of inlet velocity prescribed symmetrically at the fuel and air inlets. The axial inlet velocities were specified in the `0/U` file as equal and opposite values (± 0.1 m/s and ± 0.2 m/s), while keeping all other parameters unchanged. The inlet temperatures for both the fuel and oxidizer streams were fixed at 300 K (defined in `0/T`), and the operating pressure was maintained at 1 bar by setting the internal pressure field and outlet total pressure in the `0/P` file.

The fuel and oxidizer compositions were kept identical across all cases by prescribing the same species mass fractions in the `0/` folder and by using an unchanged Bilger mixture fraction definition in `system/FOBilgerMixtureFraction`. This ensured that any observed differences in the flame structure could be attributed solely to changes in the inlet velocity.

Each case was initialized using the same initial fields and advanced in time with the `reactingFoam` solver until a steady flame structure was achieved. After convergence, centerline temperature profiles were extracted along the axial direction using the sampling setup in `system/sample` to enable quantitative comparison of the flame response to varying inlet velocities.

3.2 Results and Discussion

Figure 3 shows the centerline temperature profiles for different inlet velocities, for the same mesh resolution Mesh B. A clear dependence of flame structure on inlet velocity is observed.

Effect on Flame Thickness and Peak Temperature

At lower inlet velocities, the flame exhibits a broader temperature profile with a relatively higher peak temperature. As the inlet velocity increases, the flame zone becomes thinner and the peak temperature decreases slightly. This behavior is attributed to the increased strain rate imposed by the opposing jets, which enhances convective transport and reduces the residence time of reactants within the reaction zone.

Flame Stabilization and Strain Effects

An increase in inlet velocity shifts the flame left towards the stagnation plane ($x \approx 0.0077$), and sharpens the temperature gradients across the flame front. At higher velocities, the stronger aerodynamic strain competes more effectively with chemical reaction rates, leading to a more compact flame structure.

These results are consistent with counterflow flame theory, where increased inlet velocities lead to thinner flames and can eventually result in flame extinction if the strain exceeds a critical value.

3.2 Results and Discussion

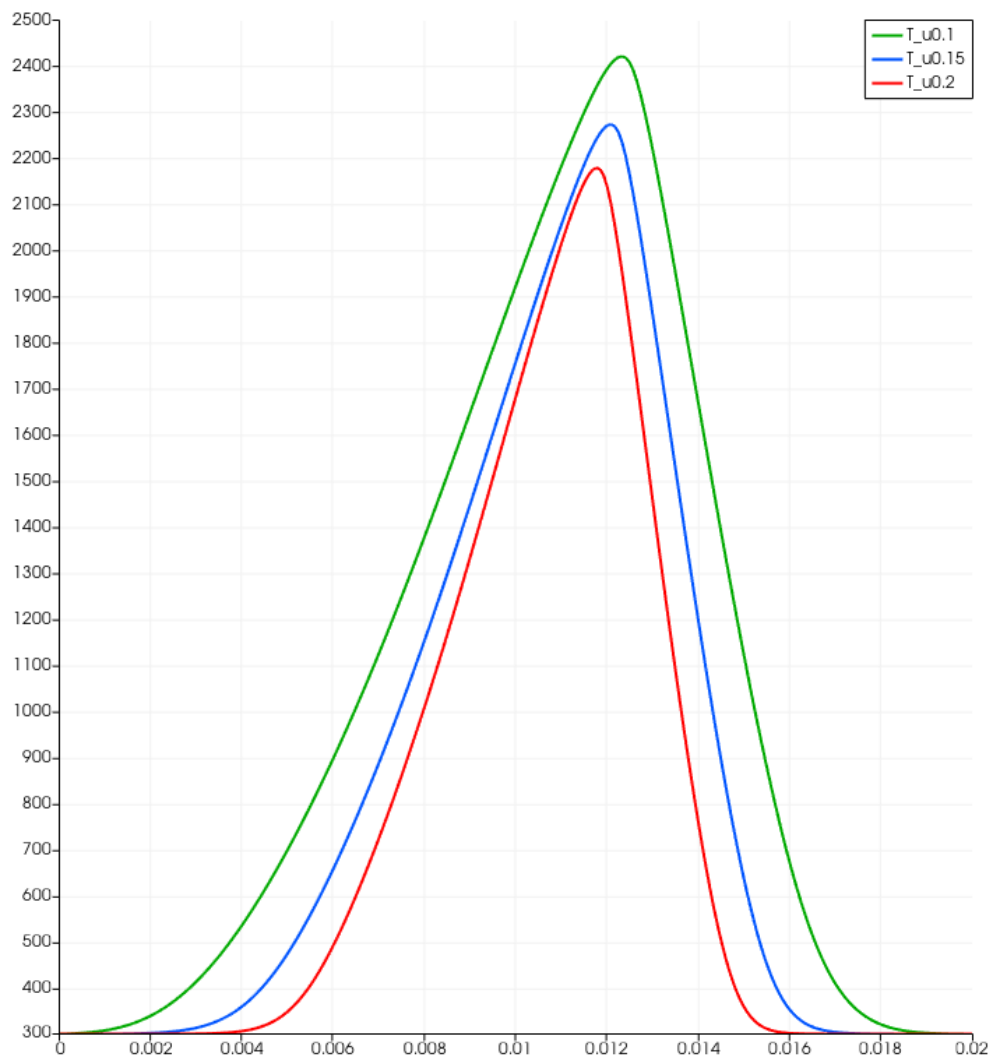


Figure 3: "Temperature vs Axial-location plot" $T(x)$ showcasing centerline temperature profiles for different inlet velocities

4 Exercise (c): Effect of Pressure

In this exercise, the influence of operating pressure on the counterflow flame structure is investigated. By increasing the operating pressure while keeping all other parameters fixed, the resulting changes in flame temperature, species distribution, and mixture fraction behavior can be systematically analyzed.

All simulations in this exercise are performed using Mesh B, as identified in Exercise (a), to ensure grid-independent results, but for fuel 2.

4.1 Simulation Steps

Two operating pressures were simulated, using fuel 2, while keeping identical cases between the below two models, so that pressure remained only varying parameter:

- Case C1: $p = 1.5$ bar,
- Case C2: $p = 4$ bar.

First, the Fuel 2 composition was prescribed at the fuel inlet by updating the species mass fractions in the respective species files in `0/species`. In addition, the Bilger mixture fraction definition in `system/FOBilgerMixtureFraction` was updated to match Fuel 2 using mole fractions.

For each pressure level, the internal pressure field and outlet total pressure were set consistently in the `0/P` file, while maintaining the same inlet velocities of ± 0.15 m/s (defined in `0/U`) and inlet temperatures of 300 K for both streams (defined in `0/T`). Each case was advanced using `reactingFoam` until a steady flame structure was obtained.

After convergence, centerline profiles of temperature and selected species (CH_4 , CO_2) were extracted along the axial direction using `system/sample`. The corresponding Bilger mixture fraction field was also sampled and plotted with python, to analyze T as a function of f_{Bilger} .

4.2 Results and Discussion

Temperature Distribution

Figure 4b shows the centerline temperature profiles obtained at different operating pressures. An increase in pressure results in a noticeable rise in the peak flame temperature, while the flame location remains close to the stagnation plane.

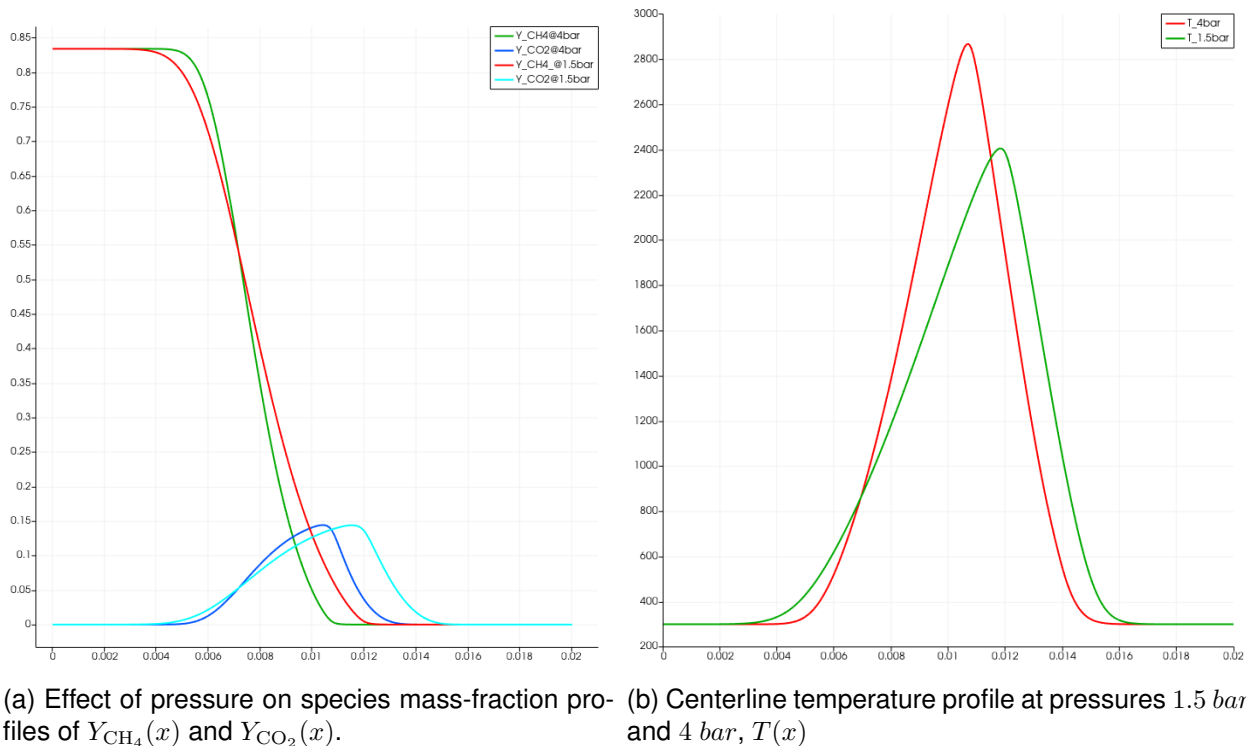
The higher peak temperature at elevated pressure can be attributed to enhanced reaction rates and reduced thermal diffusivity, which together promote more intense heat release within a narrower reaction zone.

Species Distribution

The effect of pressure on species evolution is shown in Figure 4a, which shows the centerline

4.2 Results and Discussion

mass-fraction profiles of CH_4 and CO_2 . At higher pressure, methane is consumed more rapidly, and the formation of combustion products such as CO_2 is enhanced.



(a) Effect of pressure on species mass-fraction profiles of $Y_{\text{CH}_4}(x)$ and $Y_{\text{CO}_2}(x)$. (b) Centerline temperature profile at pressures 1.5 bar and 4 bar, $T(x)$

Figure 4: Centerline temperature and mass-fraction profiles at different operating pressures.

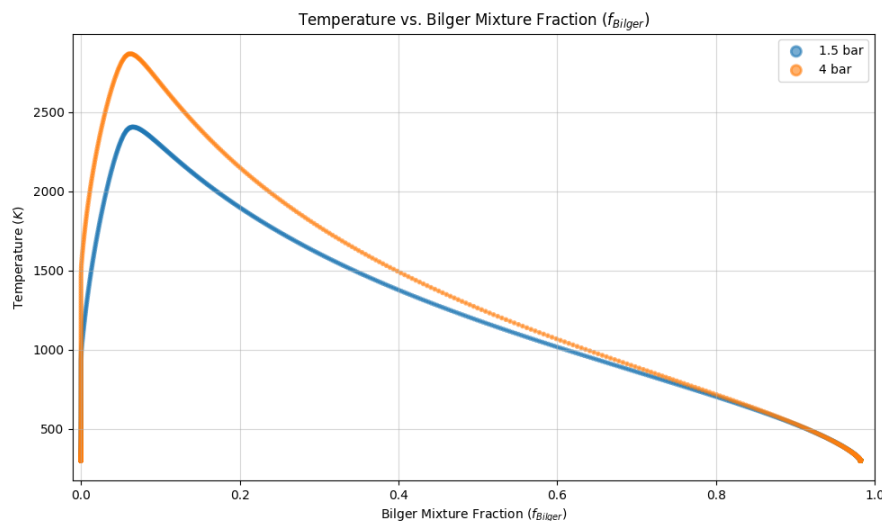


Figure 5: $T(f_{\text{Bilger}})$, Temperature as a function of Bilger mixture fraction at different operating pressures.

4.2 Results and Discussion

Mixture Fraction Analysis

Figure 5 presents the flame temperature plotted as a function of the Bilger mixture fraction. The Bilger mixture fraction depicts how mixed the fuel and air are, independent of chemistry. When temperature is plotted as a function of the Bilger mixture fraction, the flame structure collapses onto a single curve, with the temperature peaking near the stoichiometric mixture fraction. This demonstrates that the flame is mixing-controlled and that pressure primarily affects reaction intensity rather than the underlying mixing state.

As seen in the plotted result Fig. 5 the temperature peaks near the stoichiometric mixture fraction for both pressure levels, confirming that the flame structure remains controlled by local mixing rather than spatial location.

At higher pressure, the temperature curve shifts upward, indicating stronger heat release for the same mixture fraction.

Overall, the results demonstrate that increasing pressure intensifies combustion by enhancing reaction rates and product formation, while the fundamental flame structure in mixture fraction space remains unchanged.

5 Exercise (d): Effect of Fuel Inlet Temperature

In this exercise, the influence of the fuel inlet temperature on the counterflow flame structure is investigated using Fuel 3.

5.1 Simulation Steps

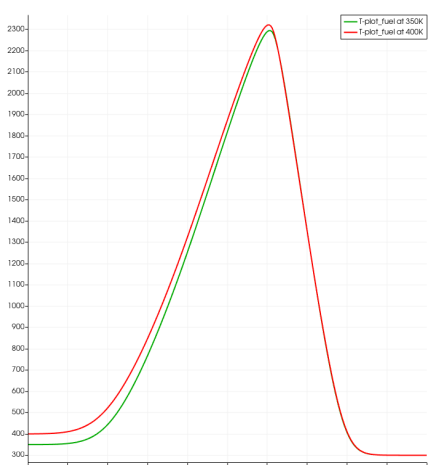
The Fuel 3 composition was prescribed at the fuel inlet using the corresponding species mass fractions in the 0/ folder, and the fuel composition for the Bilger mixture fraction was updated in *system/FOBilgerMixtureFraction* using mole fractions. The axial inlet velocities were kept constant at ± 0.15 m/s (defined in 0/U), and the operating pressure was maintained at 1 bar (defined in 0/P). While oxidiser inlet temperature is kept fixed, two simulations were performed as shown below with increased fuel inlet temperature to study how fuel preheating affects flame position, peak temperature, and flame structure in mixture-fraction space. All simulations are performed on Mesh B, following the grid-independence conclusion from Exercise (a).

Two cases were simulated:

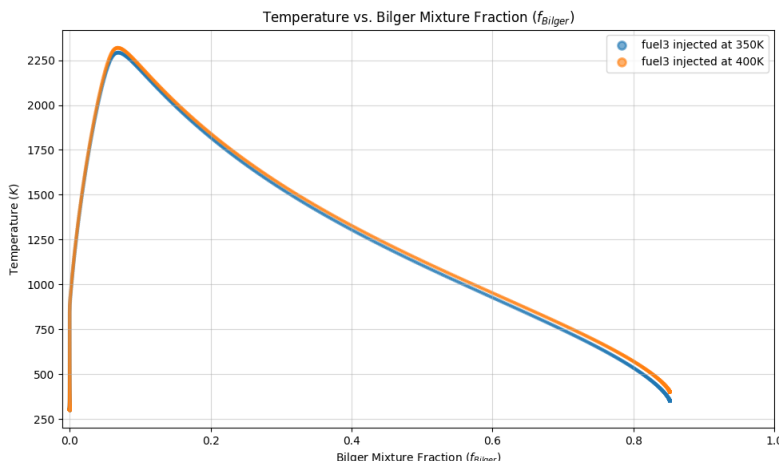
- Case D1: $T_1 = 350$ K, $T_2 = 300$ K,
- Case D2: $T_1 = 400$ K, $T_2 = 300$ K.

Each case was advanced using `reactingFoam` until a steady flame structure was obtained. After convergence, centerline profiles of temperature were extracted along the axial direction. In addition, the flame structure was analyzed in mixture-fraction space by plotting temperature as a function of the Bilger mixture fraction.

5.2 Results and Discussion



(a) Centerline temperature vs axial direction, $T(x)$.



(b) Temperature vs Bilger mixture fraction, $T(f_{\text{Bilger}})$.

Figure 6: Effect of fuel inlet temperature on the flame structure using Fuel 3.

5.2 Results and Discussion

Figure 6 compares (i) the centerline temperature profiles $T(x)$ and (ii) the temperature as a function of Bilger mixture fraction $T(f_{\text{Bilger}})$ for the two fuel inlet temperatures.

Spatial Flame Structure (Fig. 6a)

Increasing the fuel inlet temperature results in slightly higher flame temperatures. This behavior is expected, as a hotter fuel stream reduces the required sensible heating before reactions accelerate, effectively promoting earlier ignition and moving the reaction zone upstream relative to the incoming oxidizer stream. The temperature gradient across the flame zone remains steep in both cases, indicating that the flame remains thin and strain-stabilized under the present operating conditions.

Mixture Fraction Representation (Fig. 6b)

When expressed as a function of mixture-fraction space, higher inlet fuel temperature leads to higher temperature peak. Although both cases exhibit a similar temperature peak located near the stoichiometric mixture fraction, indicating that the mixing state at which maximum heat release occurs is unchanged. However, fuel preheating shifts the overall $T(f_{\text{Bilger}})$ curve upward on the fuel-rich side due to higher inlet enthalpy.

Overall, the results demonstrate that fuel preheating enhances flame reactivity and modifies the spatial flame towards the oxidiser side, but does not significantly alter the stoichiometric mixture fraction location of the peak temperature in mixture-fraction space.

6 Exercise (e): Effect of Fuel Composition at Elevated Pressure

The influence of fuel composition on flame structure and heat release is investigated at an elevated operating pressure of 1.5 bar. Three fuel mixtures (Fuel 1, Fuel 2, and Fuel 3) are compared under identical flow, thermal, and numerical settings. The objective is to quantify how fuel dilution and the presence of inert/active diluents (N_2 , H_2O , CO_2) modify (i) temperature levels, (ii) CH_4 consumption and product formation, and (iii) the heat release rate distribution along the centerline.

All simulations are performed on Mesh B, following the grid-independence conclusion from Exercise (a).

6.1 Simulation Steps

For all cases, the inlet velocities were fixed at ± 0.15 m/s (defined in $0/U$), and the inlet temperatures were set to 300 K for both streams (defined in $0/T$). The operating pressure was set to 1.5 bar by specifying the internal pressure field and outlet total pressure in $0/P$. The fuel composition was prescribed via the inlet species mass fractions in the $0/$ folder, while the Bilger mixture fraction definition in *system/FOBilgerMixtureFraction* was updated using the corresponding fuel mole fractions. The oxidizer composition (air) was kept constant in all cases.

Each case was simulated with `reactingFoam` until a steady flame structure was obtained. After convergence, centerline profiles of temperature, selected species (CH_4 , CO_2 , H_2O), and heat release rate (\dot{Q}) were extracted for comparison.

6.2 Results and Discussion

Temperature Levels (Fig. 7)

The temperature profiles differ across the fuels due to dilution and thermal effects. Fuel 1 (dilution by N_2) exhibits the highest peak temperature among the three cases, whereas fuels containing CO_2/H_2O show reduced peak temperature. Then followed by Fuel 3 (diluted by CO_2 and H_2O). This reduction is consistent with the higher heat capacity of CO_2 and H_2O , which increases sensible enthalpy requirements and thus lowers adiabatic flame temperature.

Heat Release Rate Distribution (Fig. 8)

The heat release rate profiles reveal that Fuel 1 produces the strongest and most localised heat release peak, compared to Fuel 2 and Fuel 3. The presence of CO_2 and H_2O in Fuel 2/Fuel 3 broadens the heat release region slightly and lowers the peak magnitude, indicating a less intense reaction zone. This behaviour is expected as diluents reduce reactant concentrations and increase the mixture heat capacity, both of which decrease peak reaction intensity.

Overall, the results demonstrate that fuel dilution significantly influences flame temperature and heat release intensity. Inert dilution (N_2) primarily reduces reactant concentration without strongly increasing heat capacity, whereas dilution with H_2O and CO_2 introduces stronger thermal damping effects, leading to lower peak temperatures and reduced heat release rates.

6.2 Results and Discussion

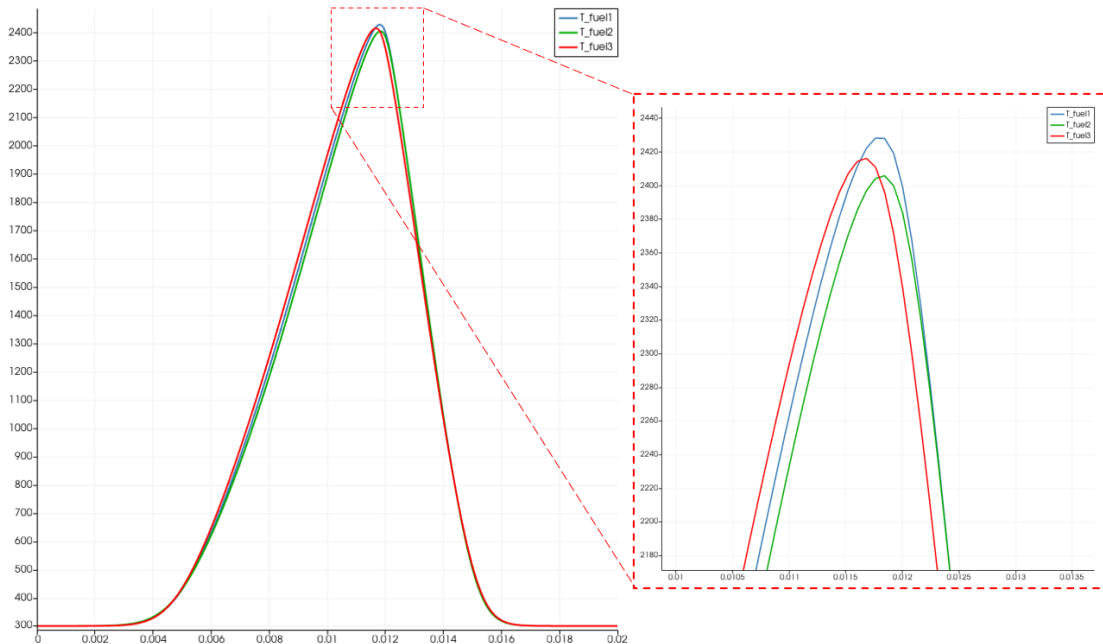


Figure 7: Centerline temperature profiles, $T(x)$.

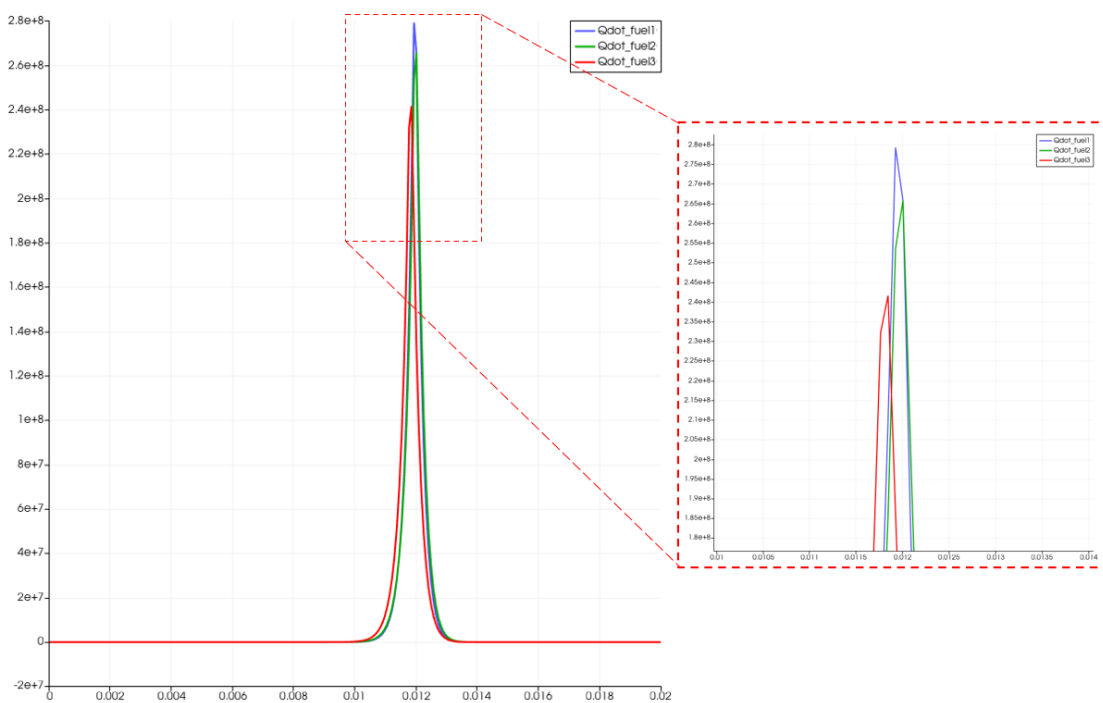


Figure 8: Centerline heat release rate, $\dot{Q}(x)$.

Methane Consumption and Product Formation (Fig. 9)

The methane mass fraction decreases sharply through the reaction zone in all cases, indicating rapid fuel consumption near the flame front. Fuel 2 and Fuel 3, which include H_2O and/or CO_2 dilution, show slightly smoother gradients and altered downstream product levels.

In particular, Fuel 3 exhibits a higher initial CO_2 level due to its inlet dilution, while its net CO_2 formation in the reaction zone reflects the combined effect of inlet composition and combustion chemistry. The H_2O profiles similarly capture both inlet contribution (for fuel 2/fuel 3) and additional product formation due to oxidation.

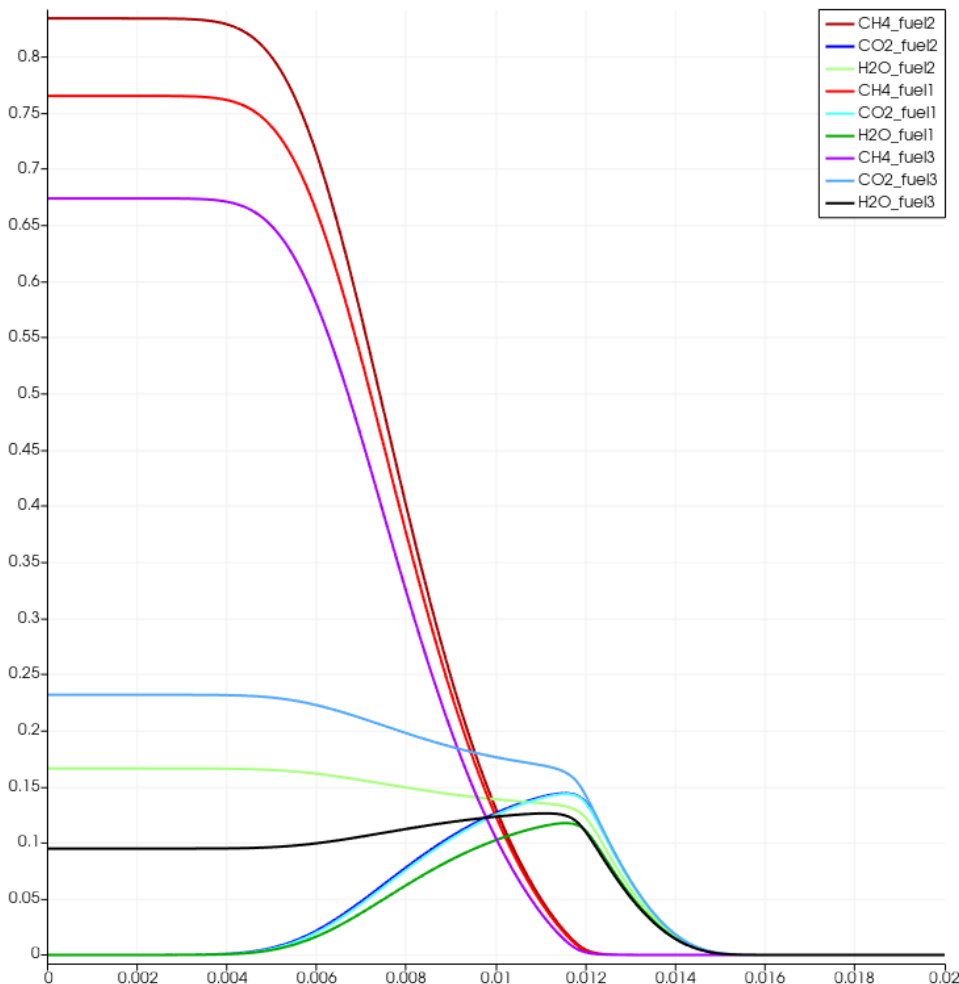


Figure 9: Mass-fraction, $Y_{CH_4}(x)$, $Y_{CO_2}(x)$ and $Y_{H_2O}(x)$ for fuel 1, fuel 2, and fuel 3.

7 References

1. Detailed OpenFOAM simulation files and source data are available in this: [GitHub Repository](#)